Flexible radiofrequency filters based on highly conductive graphene assembly films

Wenqing Zhou, Chengguo Liu, Rongguo Song, Xianci Zeng, Bao-Wen Li, Wei Xia, Jingwei Zhang, Guan-Long Huang, Zhi Peng Wu, and Daping He (iD)

View Online   Export Citation   CrossMark

Applied Physics Reviews
Now accepting original research

2017 Journal
Impact Factor:
12.894

AIP
Publishing

Flexible radiofrequency filters based on highly conductive graphene assembly films

View Online   Export Citation   CrossMark

Wenqing Zhou,[1] Chengguo Liu,[1] Rongguo Song,[1] Xianci Zeng,[1] Bao-Wen Li,[2] Wei Xia,[1] Jingwei Zhang,[1] Guan-Long Huang,[3] Zhi Peng Wu,[1] and Daping He[1,2,a] (ID)

AFFILIATIONS

[1]Hubei Engineering Research Center of RF-Microwave Technology and Application, Wuhan University of Technology, Wuhan 430070, China

[2]State Key Laboratory of Advanced Technology for Materials Synthesis and Processing, Wuhan University of Technology, Wuhan 430070, China

[3]ATR National Key Laboratory of Defense Technology, College of Information Engineering, Shenzhen University, Shenzhen, Guangdong 518060, People's Republic of China

[a]Author to whom correspondence should be addressed: hedaping@whut.edu.cn

ABSTRACT

We demonstrate a flexible radiofrequency filter based on graphene assembly films with a high conductivity up to 10^6 S/m and a thickness of $10\,\mu m$. The flexible high-conductivity graphene film (HCGF) used in the filter has a fifth-order low-pass Chebyshev frequency response, and it operates at 3.6 GHz with a 0.82 dB in-band maximum insertion loss and 26.21 dB insertion loss at 5 GHz. Such performance observed in the HCGF-based flexible filters is comparable to that of commercial copper-based filters in passband and roll-off. The HCGF exhibits good mechanical flexibility even after 200 cycles of bending. Nearly no mechanical failure or performance degradation occurs during 20 cycles of $0°-50°$ bending for the flexible HCGF filter. Our results suggest that the flexible HCGF filter has good repetitive bending stability. This makes this type of filter suitable for future applications in flexible wireless communication.

Published under license by AIP Publishing. https://doi.org/10.1063/1.5074172

The development of flexible electronics offers benefits in a wide-variety of potential applications. Major advantages over conventional rigid electronics are in weight, volume, and portability. More specifically, flexible devices can be used in areas such as portable displays, conformable radio frequency identification (RFID) tags, and wearable health care.[1–3] Therefore, wireless communication systems based on flexible electronics have received considerable attention over the recent years. Flexible components have been explored for modern wireless communication systems, such as antennas, transmission lines, filters, and inductors.[4–7] However, the study of high-performance flexible filters for suppressing spurious signals and interferences in the wireless communication systems is far less explored and still an active subject for research.[8]

Introducing flexibility into commercial filters has been attempted by adoption of flexible substrates, such as liquid crystal polymers (LCP), LCP copper clad substrates, and polydimethylsiloxane (PDMS).[9–11] These proposed materials with good mechanical flexibility can be fabricated from a low-temperature process, although the conductor strips of filters are still based on traditional rigid solid metals. To achieve the flexibility of conductor strips, liquid metal has been used.[12,13] However, the fabrication process is quite complicated and difficult to control accurately. Therefore, a flexible material for convenient fabrication will be the driving force to promote the development of flexible filters.

Graphene is a very promising material for wireless wearable communication applications owing to its high conductivity and other unique properties. In previous reports, graphene-based filters have demonstrated good performances in Terahertz frequencies, including stepped impedance low-pass,[14] flat-top band-pass,[15] and band-stop graphene filters,[16] while those in microwave frequencies have barely been covered so far. This is because the graphene filter is generally based on monolayer graphene, which has a high sheet resistance and relatively low conductivity,[17,18] causing large insertion losses in the microwave band. On the other hand, in our previous work, we have reported that graphene assembly films consisting of multilayer graphene nanosheets have low sheet resistance and excellent planar conductivity.[19] Moreover, flexible high-conductivity graphene films (HCGFs) exhibit better mechanical toughness and flexibility than

traditional rigid solid metal films, as well as offering an easier process of production compared to that for liquid metal processes. These properties make the HCGF a perfect candidate for flexible microwave filters with high performance.

In this paper, we demonstrate a flexible low-pass filter (LPF) based on the HCGF material. The flexible LPF operates at 3.6 GHz with 0.82 dB in-band maximum insertion loss and 26.21 dB insertion loss at 5 GHz. Added stubs are designed to extend the 20 dB rejection stopband from 5 GHz to more than 12 GHz. Significantly, the proposed filter is insensitive to bending deformation, since there are no signs of degradation in both structural integrity and performance of the filter after having been repeatedly bend with different angles and times.

The HCGF was fabricated by the following steps. First, a graphene oxide (GO) suspension was diluted with ultrapure water to obtain a GO aqueous solution with a concentration of 15 mg/ml. Thereafter, the diluted GO aqueous solution was dropped on a polyethylene terephthalate (PET) film and then evaporated at room temperature to obtain the GO assembly films.[20] Second, the GO assembly films were annealed at 1300 °C for 2 h and then at 2850 °C for 1 h in an argon (Ar) gas flow environment. Finally, the HCGF quality was achieved by a rolling compression process. Figure 1(a) shows the photograph of the HCGF indicating excellent flexibility. Scanning electron microscopy [SEM; Fig. 1(b)] shows that HCGF is based on an assembly or ordered stack of graphene layers with a total thickness of ~10 μm. Figure 1(c) shows the X-ray diffraction (XRD) pattern of the HCGF. The characteristic graphitic peak is located at $2\theta = 26.5°$, which indicates that the HCGF has a regular packing of graphene layers and with an interlayer spacing (002) of ~0.34 nm. A schematic diagram is shown in the inset of Fig. 1(c). The strong intensity of the diffraction peak (004) indicates a high degree of graphitization and order in the HCGF material. Figure 1(d) illustrates the mechanical stability of the HCGF material. The HCGF material and wires were fixed with two insulated clamps. Electrical resistance was measured by using a digital multimeter (Agilent U1242B). After 200 cycles of bending tests with bending speeds of 2 Hz and bending degrees of 0° (initial
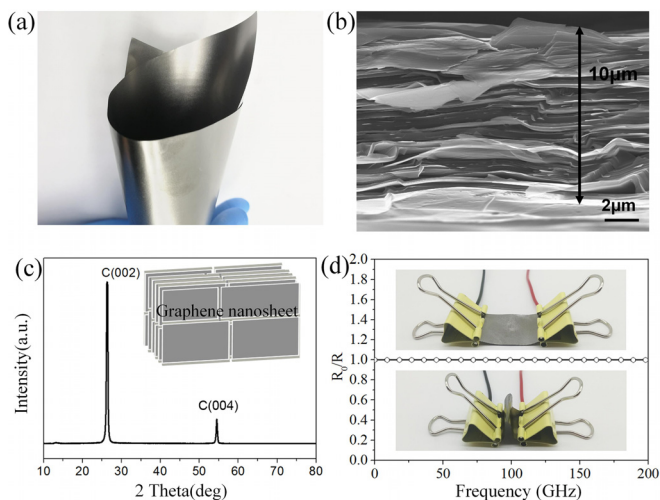
state) and 80° (bend state), the relative volume resistance of the HCGF almost remains constant.

The specifications for the LPF under consideration are as follows: the filter has a low-pass Chebyshev frequency response with a 3 dB cut-off frequency of 3.6 GHz and a very wide rejection band, and the out-of-band insertion loss at 5 GHz is expected to be higher than 20 dB. According to these requirements and the normalized frequency curve of a Chebyshev filter,[21] the fifth-order low-pass prototype with Chebyshev response is chosen. Discrete inductance (L) and capacitance (C) values are shown in Fig. 2(a) and can be calculated using the following equations:

$$L_2 = L_4 = \frac{Z_0 g_2}{2\pi f_c} = \frac{Z_0 g_4}{2\pi f_c}, \tag{1}$$

$$C_1 = C_5 = \frac{g_1}{Z_0 2\pi f_c} = \frac{g_5}{Z_0 2\pi f_c}, \tag{2}$$

$$C_3 = \frac{g_3}{Z_0 2\pi f_c}. \tag{3}$$

Here, the normalized element values are[22] $g_0 = g_6 = 1$, $g_1 = g_5 = 1.7058$, $g_2 = g_4 = 1.2296$, $g_3 = 2.5408$, $Z_0 = 50 \, \Omega$, and f_c is the cut-off frequency. When the circuit is implemented using a microstrip line, the series inductance can be replaced by a high impedance line. A shunt capacitor is realized with an open-circuited stub. The lengths of high-impedance lines (l_L) and open-circuited stub (l_C) are obtained, respectively, using the following equations:

$$l_C = \frac{\lambda_{gC}}{2\pi} \tan^{-1}(2\pi f_c Z_{0C} C), \tag{4}$$

$$l_L = \frac{\lambda_{gL}}{2\pi} \sin^{-1}\left(\frac{2\pi f_c L}{Z_{0L}}\right). \tag{5}$$

FIG. 1. (a) Photograph showing the graphene film. (b) Cross-sectional SEM image. (c) XRD pattern and a schematic diagram of the ordered stacking structure (inset). (d) Photograph showing stability testing for the HCGF.
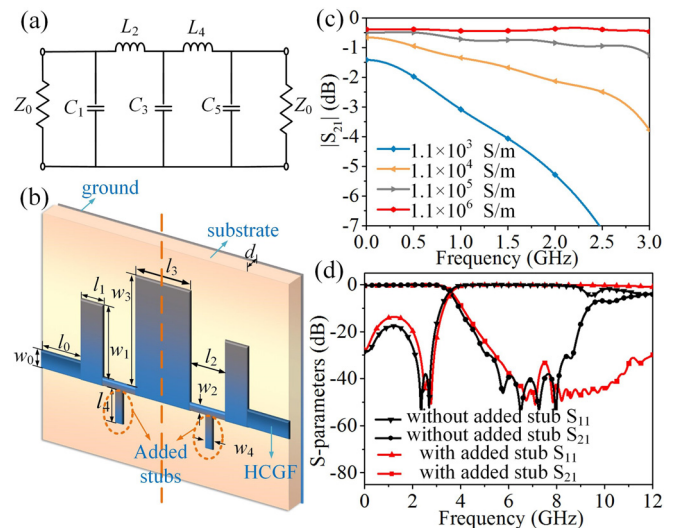

FIG. 2. The design of the HCGF filter. (a) The circuit diagram. (b) The 3D geometric model of the HCGF filter, $w_0 = 2.42$ mm, $w_1 = 9.10$ mm, $w_2 = 0.40$ mm, $w_3 = 10.00$ mm, $w_4 = 1.00$ mm, $l_0 = 10.00$ mm, $l_1 = 3.10$ mm, $l_2 = 4.20$ mm, $l_3 = 5.60$ mm, and $l_4 = 5.00$ mm. (c) Insertion losses of the filter for various conductivities of the filter (σ). (d) The simulated $|S_{11}|$ and $|S_{21}|$ responses of the designed filter with and without added stubs.

Here, λ_{gC} and λ_{gL} are the dielectric wavelength of inductance and the dielectric wavelength of capacitance, respectively. The characteristic impedance of the high-impedance lines (Z_{0L}) is set as 110 Ω, while the characteristic impedance of open-circuited stub (Z_{0C}) is chosen as 15 Ω.

Based on the filter obtained by the above method, the transmission zero point is obtained by parallel added stubs on the high impedance line, which allows realization of a better stop-band response.[23] The electrical length of the open-circuited stub is calculated using the following equation:

$$\beta l_5 = (2k+1)\frac{\pi}{2}. \qquad (6)$$

In the simplest case, $k = 0$ and β is the phase change constant, which is $2\pi/\lambda_0$. The lengths (l_1, l_2, l_3, l_4, and l_5) and widths (w_1, w_2, w_3, w_4, and w_5) of the microstrip line sections can be obtained, as shown in Fig. 2(b).

The design process of the HCGF based filter is demonstrated in Figs. 2(a) and 2(b), which display the circuit diagram and the 3D geometric model of the flexible LPF, respectively. The LPF consists of three layers, including the HCGF conductor strip, substrate, and ground from top to bottom. In addition, the outline of the LPF consists of two 50 Ω lines at two sides, five low- and high-impedance lines in the middle, and two added stubs on both sides. To ensure the best effect of the filter, the calculated values are optimized by simulation. The flexible LPF is fabricated on a Ro5880 substrate with a relative permittivity ε_r of 2.2 and a thickness d of 0.787 mm. Figure 2(c) shows the insertion loss of the LPF for various conductivities σ of the graphene film. The values of conductivity are set to 1.1×10^3 S/m, 1.1×10^4 S/m, 1.1×10^5 S/m, and 1.1×10^6 S/m. The insertion losses in the passband increase with the decrease in σ, which is mainly caused by the conductive losses. The corresponding insertion losses at 2 GHz deteriorates from 0.36 dB to 0.85 dB, 2.15 dB, and 5.28 dB. Figure 2(d) shows the simulated results of the proposed filter with and without parallel added stubs. It can be observed that the stopband enormously broadens with the parallel added stubs, which can be extended from 5 GHz to more than 12 GHz, and higher-order harmonics are suppressed. Besides, the parallel added stubs do not affect the $|S_{11}|$ of the filter.

The surface current distributions of the HCGF filter at 2 GHz and 5 GHz are shown in Figs. 3(a) and 3(b), respectively. In the passband at 2 GHz, low loss propagation of the signal can be realized using the HCGF filter. In the stopband, the electric signal at 5 GHz is restrained inside the low-pass filter. These results show the effective selectivity of signal propagation in the passband and stopband. The proposed filter is measured with a Network Analyzer (PNA, Keysight N5247A). Under flat circumstances, the simulated and measured S-parameters of filters are shown in Figs. 3(c) and 3(d). There is good agreement between the simulated and measured results. Figures 3(c) and 3(d) show that two poles of $|S_{11}|$ and transmission zeros of $|S_{21}|$ are generated for providing the expected bandpass characteristics and sharp frequency response, and it has a maximum insertion of up to 0.82 dB in the passband. The measured result of out-of-band insertion loss is 26.21 dB at 5 GHz, which meets the design requirements. The LPF shows good stopband effects indicating that a 20 dB rejection stopband can be extended to more than 12 GHz, as shown in Fig. 3(d). To further study the flexibility properties of the LPF, we repeatedly
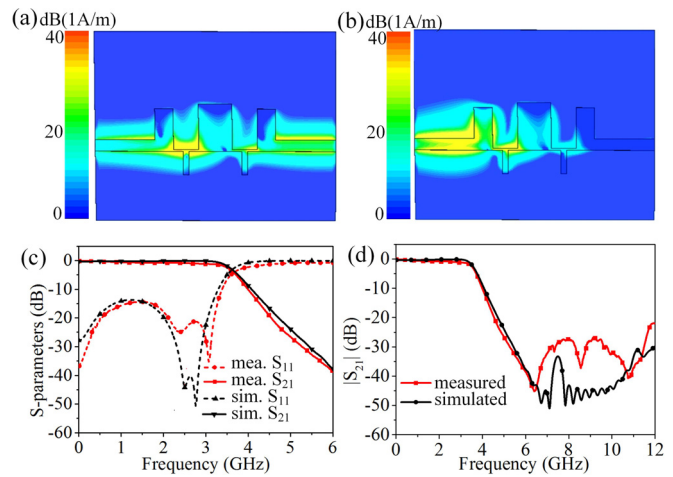

FIG. 3. (a) The simulated current distribution of the filter in the passband. (b) The simulated current distribution of the filter in the stopband. (c) Simulated and measured S-parameters for the filter. (d) $|S_{21}|$ responses for the filter.

bend the filter along the X axis at an angle of θ as shown in Fig. 4(a). Figure 4(b) shows the prototypes of filters with different angles. We compared $|S_{11}|$ and $|S_{21}|$ responses between the flat condition (0°) and the bend condition (10°, 20°, 30°, 40°, and 50°) in Figs. 4(c) and 4(d). The $|S_{11}|$ results show that the minimum return losses in flat conditions are 14.31 dB, and the change in values of the minimum return loss from angles of 10°, 20°, 30°, 40°, and 50° is 0.7 dB, 1.67 dB, 0.40 dB, 1.12 dB, and 0.28 dB, respectively. The two poles of $|S_{11}|$ are basically unchanged, which are around 2.3 GHz and 3.1 GHz in Fig. 4(c). The measured results of cutoff frequency at 0°–50° are almost around 3.6 GHz in Fig. 4(d). Compared with the flat condition, when folded angle θ is altered to the aforementioned values, the
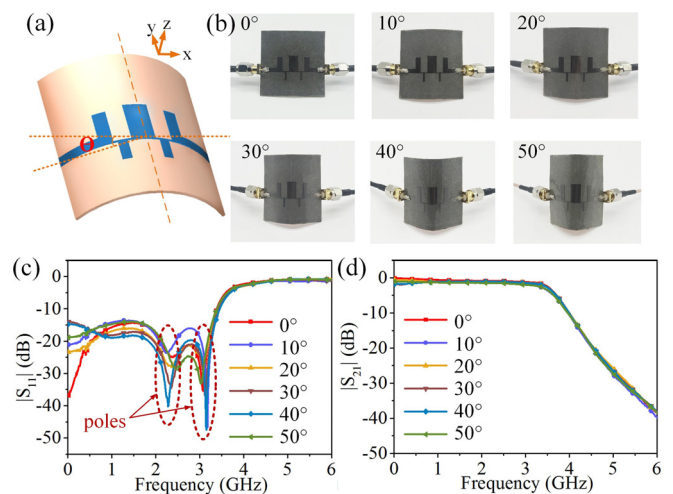

FIG. 4. (a) Drawing to illustrate the flexibility property of the HCGF filter and the model of filter bending. (b) Photographs showing the prototypes of filters with different bend angles. (c) $|S_{11}|$ responses of the filter for various angles. (d) $|S_{21}|$ responses of the filter for various angles.
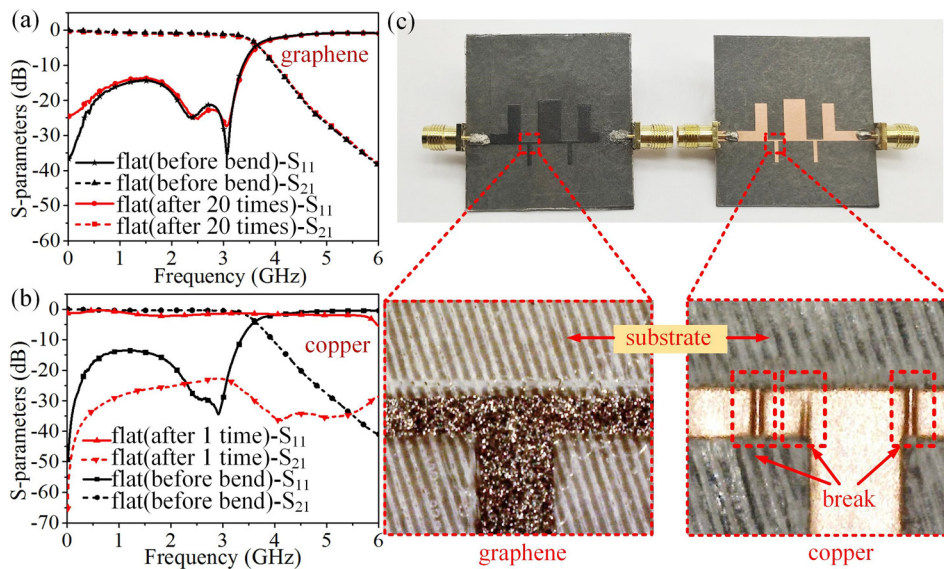
FIG. 5. (a) Measured S-parameters for the HCGF filters in a flat state and after 20 cycles of fatigue testing, (b) Measured S-parameters for the copper filter after 1 cycle of fatigue testing, (c) Photographs showing HCGF and copper filters after the bending test.

corresponding maximum insertion loss is increased by 0.27 dB, 0.21 dB, 0.12 dB, 0.29 dB, and 0.63 dB, respectively, in Fig. 4(d). Compared with flat conditions, there are very small changes of the $|S_{11}|$, $|S_{21}|$, cutoff frequency, and poles. Therefore, the proposed LPF made by HCGF shows excellent flexibility, which can still maintain good performance during bending cycles.

To further investigate the stability of HCGF LPF, a copper filter with the same size was fabricated. Figure 5(a) shows the measured $|S_{11}|$ and $|S_{21}|$ of the HCGF filter in the flat state, bent at 50° and then restored to 0° for 20 times. The result shows that the curve of bending 20 times overlaps with the curve when unbent, indicating that the stability performance of the flexible filter is well preserved. Figure 5(b) shows the same fatigue testing for the copper filter. The values of $|S_{21}|$ of the copper filter are all under the 20 dB after bending only 1 time, which means that the copper filter is performing poorly. The loss of performance for the traditional copper filter mainly results from metal fatigue. Figure 5(c) shows prototypes of graphene and copper filters and their partially enlarged drawing. The labeled microstrip line is magnified 30 times and observed by optical microscopy. It is shown that progressive and localized structural damage occurs when copper is subjected to cyclic loading. Once the load is above a threshold for copper, microscopic cracks begin to form at grain interfaces, and the structure starts to fracture.[24] In Fig. 5(c), there are several obvious breaks in the microstrip line of the filter, which leads to the failure of the filter. However, the surface of graphene is still smooth and intact even after 20 cycles of repetitive bending. The stability of the graphene filter was significantly improved compared with that of the traditional copper filter, which will substantially increase the service life of the flexible filter.

In summary, a flexible microstrip low-pass filter based on HCGF is investigated and verified through simulation and measurement. The flexible filter operates at 3.6 GHz with 0.82 dB in-band maximum insertion losses and it possesses 26.21 dB insertion losses at 5 GHz. Added stubs are applied to realize a wider stopband for extending the 20 dB rejection stopband beyond 12 GHz. The designed filter exhibits insensitivity to bending. Compared with the traditional copper film devices, the HCGF filter keeps surface smoothness and remains intact after repeated bending, while obtaining better durability and mechanical flexibility. The proposed filter has potential for applications in 5 G communication systems as well as in wearable and implantable electronics.

REFERENCES

[1] J. Zhao, S. Wang, H. Wu, Y. Liu, Y. Chang, and X. Chen, Appl. Phys. Lett. 110, 094108 (2017).
[2] S. Chun, Y. Kim, H. Jung, and W. Park, Appl. Phys. Lett. 105, 041907 (2014).
[3] X. Huang, T. Leng, X. Zhang, J. Chen, K. Chang, A. K. Geim, K. S. Novoselov, and Z. Hu, Appl. Phys. Lett. 106, 203105 (2015).
[4] X. Yang, A. Vorobiev, A. Generalov, M. A. Andersson, and J. Stake, Appl. Phys. Lett. 111, 097105 (2017).
[5] R. Song, Q. Wang, B. Mao, and Z. Wang, Carbon 130, 164 (2018).
[6] L. Sun, G. Qin, H. Huang, H. Zhou, N. Behdad, W. Zhou, and Z. Ma, Appl. Phys. Lett. 96, 013509 (2010).
[7] M. Hayati, S. Zarghami, and A. H. Kazemi, IEEE Trans. Compon. Packag. Manuf. Technol. 8, 21632170 (2018).
[8] Y. Jiang and Y. Zhao, Small 14, 1703644 (2018).
[9] M. Zhao, Y. Zhang, S. Liu, and Y. Jia, Microwaves Opt. Technol. Lett. 59, 194 (2017).
[10] J. S. Kim, K. B. Lee, J. Y. Lee, H. J. Lee, and H. Shin, Microwave Opt. Technol. Lett. 54, 384 (2012).
[11] R. Li, Y. Guo, W. Chen, Y. Li, A. Voon-Yew Thean, and Aaron, Int. J. RF Microwave Comput. Aided Eng. 28, e21265 (2018).
[12] G. Mumcu, A. Dey, and T. Palomo, IEEE Microwave Wireless Compon. Lett. 23, 187 (2013).
[13] N. Vahabisani, S. Khan, and M. Daneshmand, IEEE Microwave Wireless Compon. Lett. 26, 801 (2016).
[14] D. Correas-Serrano, J. S. Gomez-Diaz, J. Perruisseau-Carrier, and A. Alvarez-Melcon, IEEE Trans. Nanotechnol. 13, 1145 (2014).

[15]H. Deng, Y. Yan, and Y. Xu, IEEE Photonics Technol. Lett. **27**, 11611164 (2015).

[16]Z. Zhang, Y. Long, P. Ma, and H. Li, Nanotechnology **28**, 475205 (2017).

[17]J. S. Gómez-Díaz, J. Perruisseau-Carrier, P. Sharma, and A. Ionescu, J. Appl. Phys. **111**, 114908 (2012).

[18]O. Shaforost, K. Wang, S. Goniszewski, M. Adabi, Z. Guo, S. Hanham, J. Gallop, L. Hao, and N. Klein, J. Appl. Phys. **117**, 024501 (2015).

[19]Z. Wang, B. Mao, Q. Wang, J. Yu, J. Dai, R. Song, D. He, P. Z. Wu, and S. Mu, Small. **14**, e1704332 (2018).

[20]D. Tang, Z. Wang, Q. Wang, Q. Liu, B. Zhang, D. He, Z. Wu, and S. Mu, Sci. Bull. **63**, 574579 (2018).

[21]J. S. Hong and M. J. Lancaster, *Microstrip Filters for RF/Microwave Applications* (Wiley, New York, 2001), p. 113.

[22]D. M. Pozar, *Microwave Engineering* (Wiley, New York, 2011), p. 406.

[23]C. Quendo, E. Rius, and C. Person, IEEE Trans. Microwave Theory Tech. **51**, 734 (2003).

[24]W. H. Kim and C. Laird, Acta Metall. **26**, 789 (1978).